Surface plasmon assisted electron acceleration in photoemission from gold nanopillars

Phillip M. Nagel,[1,2] Joseph S. Robinson,[3] Bruce D. Harteneck,[4]
Thomas Pfeifer,[1,2,5] Mark J. Abel,[1,2,6] James S. Prell,[1]
Daniel M. Neumark,[1,2] Robert A. Kaindl,[3,*] and Stephen R. Leone[1,2,7,†]

[1]*Department of Chemistry, University of California, Berkeley, CA 94720, USA*
[2]*Ultrafast X-Ray Science Laboratory, Chemical Sciences Division, Lawrence Berkeley National Laboratory, Berkeley, CA 94720, USA*
[3]*Materials Sciences Division, Lawrence Berkeley National Laboratory, Berkeley, CA 94720, USA*
[4]*Molecular Foundry, Lawrence Berkeley National Laboratory, Berkeley, CA 94720, USA*
[5]*Max-Planck-Institut für Kernphysik, Saupfercheckweg 1, 69117 Heidelberg, Germany*
[6]*Abteilung Molekülphysik, Fritz-Haber-Institut der Max-Planck-Gesellschaft, Faradayweg 4-6, 14195 Berlin, Germany*
[7]*Department of Physics, University of California, Berkeley, CA 94720, USA*

Abstract

Electron photoemission from lithographically prepared gold nanopillars using few-cycle, 800 nm laser pulses is measured. Electron kinetic energies are observed that are higher by up to tens of eV compared to photoemission from a flat gold surface at the same laser intensities. In addition, ionization from the nanopillar sample scales like a two-photon process, while three photons are needed to overcome the work function taking into account the shortest wavelength within the laser bandwidth. A classical electron acceleration model consisting of nonlinear ionization followed by field acceleration qualitatively reproduces the electron kinetic energy data and suggests average enhanced electric fields due to the nanopillars that are between 25 and 39 times greater than the experimentally used laser fields. Implications for plasmon-enhanced attosecond streaking are discussed.

PACS numbers:

I. INTRODUCTION

Among the most intriguing phenomena in nanoscale materials today is the coherent electronic excitation in metals known as the surface plasmon resonance (SPR). The SPR is a collective oscillation of conduction band electrons that typically occurs at optical frequencies in noble metals[1]. For a short amount of time, these electrons oscillate in phase with each other and create a strongly enhanced electric field at the surface of the metal/vacuum or metal/dielectric interface[2,3]. SPRs have enormous potential for applications in medicine, communications, and electronics[4,5], most of which take advantage of the strongly enhanced electric field created by the plasmon at the metal surface. Techniques such as surface-enhanced Raman spectroscopy exploit this near field enhancement to allow the sensitive spectroscopic detection of single molecules[6].

One area of significant interest is the plasmon response to excitation by high intensity, ultrafast laser pulses. Lasers that generate such pulses are becoming increasingly common and have opened the door to studying new regimes of light/matter interactions. The goal of the present work is to investigate the interactions of laser-ionized photoelectrons with localized surface plasmon electric fields excited in a lithographically prepared nanostructured array. The use of a nanostructured surface is advantageous because the SPRs are excited directly by ultrafast laser pulses without requiring special excitation geometries often used in studies of plasmon enhanced photoemission from flat gold surfaces[7–14] or extremely sharp metal tips[15,16]. By measuring photoelectron kinetic energy spectra and electron yields as a function of laser excitation intensity, we observe photoelectron kinetic energies tens of eV higher than expected based on the laser excitation intensity. A classical electron acceleration calculation is used to model the data and to determine the average field enhancement from the nanostructures. Implications for possible studies of plasmon-enhanced attosecond photoelectron streaking are also briefly discussed.

II. EXPERIMENTAL

A. Apparatus

The measurements use a few-cycle femtosecond, visible-infrared laser pulse to excite a SPR in a lithographically prepared gold nanopillar sample and to simultaneously ionize

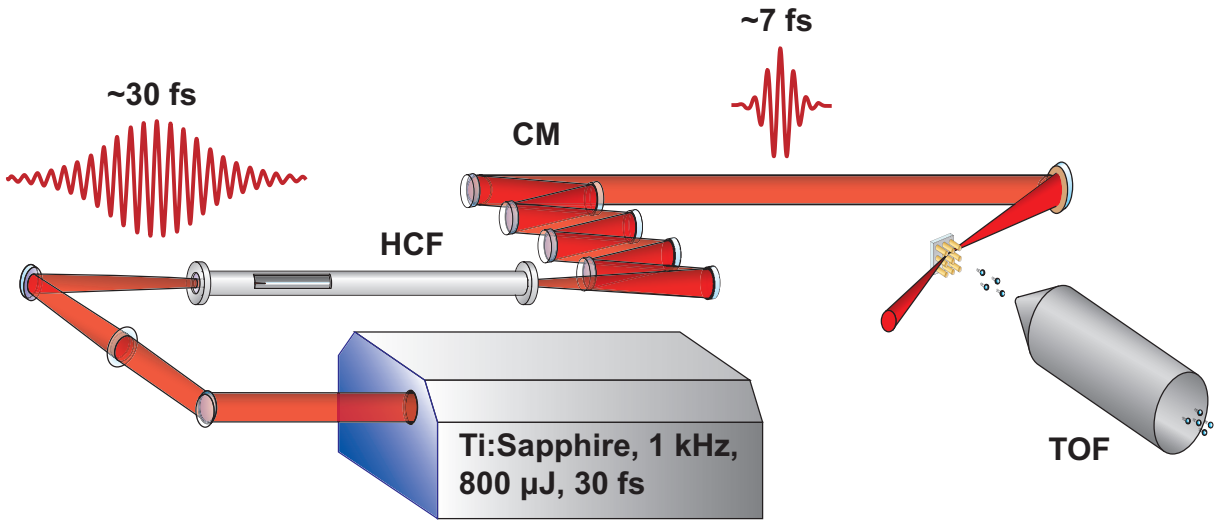

FIG. 1: Schematic of the experimental apparatus. 30 fs FWHM, 800 μJ laser pulses are spectrally broadened in a gas-filled hollow-core fiber (HCF) and temporally compressed to ≈7 fs FWHM with a series of multilayer chirped mirrors (CM). The laser is focused onto the sample surface and photoelectrons are detected using a linear time-of-flight spectrometer (TOF).

photoelectrons from the sample surface. Photoelectron kinetic energies are measured as a function of excitation intensity using a linear time-of-flight (TOF) electron spectrometer. A schematic of the experimental apparatus is shown in Figure 1.

The apparatus consists of a Femtolasers Femtopower Compact Pro multi-pass amplified Ti:Sapphire laser system that produces ≈30 fs full-width at half-maximum (FWHM), 800 μJ laser pulses at a repetition rate of 1 kHz. A 1 m long, 250 μm inner diameter hollow core glass fiber filled with 1.9 Bar of Ne gas is used for spectral broadening through self-phase modulation followed by temporal compression with a series of negatively chirped mirrors to a pulse duration of ≈7 fs FWHM. The laser spectrum extends from 540 nm to 930 nm (1% level of intensity). The laser pulse is focused at grazing incidence using a near-normal incidence spherical mirror with a high reflectivity gold coating and a 10 cm focal length to a spot size of approximately 60 μm ($1/e^2$ diameter). A 75° angle of incidence and p-polarization were chosen in order to excite the plasmon resonance along the TOF axis, and thus accelerate electrons in the direction of the TOF. The grazing angle stretches the spot size along the direction of propagation to ≈230 μm. The sample is housed in vacuum at a pressure of $< 5 \times 10^{-7}$ Torr. No steps were taken to clean the sample surface. Emitted photoelectrons are detected normal to the sample surface by the field-free TOF electron

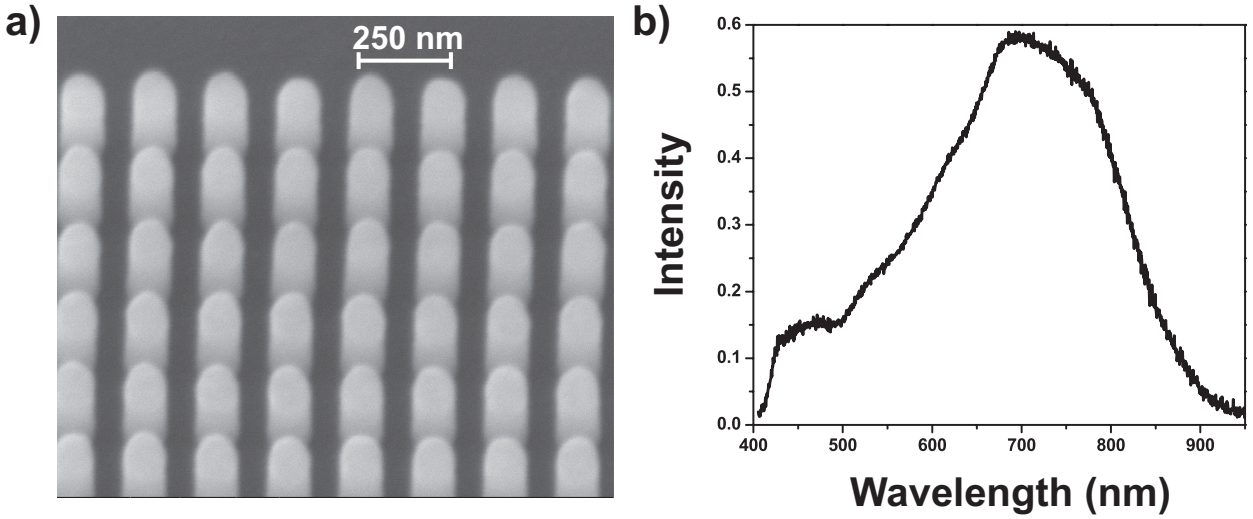

FIG. 2: (a) Scanning electron microscope (SEM) image of the gold nanopillar array. (b) Dark-field scattering measurement of a single nanopillar from an identically prepared sample with a larger pitch to allow for measurement of a single particle.

spectrometer using a micro-channel plate (MCP) detector. The acceptance angle of the spectrometer is 2° and the total flight length is 0.59 m. Signal pulses from the MCP are processed by an analog constant-fraction discriminator to correct for the MCP pulse height distribution and then counted with a digital multi-channel scaler with 500 ps resolution. The energy resolution of the TOF spectrometer varies with electron kinetic energy, ranging from ≈11 meV for 5 eV electrons to ≈1 eV for 100 eV electrons. At the count rates present in this experiment, the probability of missing an electron count during the detection electronics pulse-pair resolution dead-time ranges from 0.2% at the lowest count rates to 10% at the highest count rates. p-Polarized light is used throughout this experiment to excite SPRs normal to the sample surface and parallel to the TOF axis.

B. Nanopillar Sample

The sample investigated consists of free-standing gold nanopillars attached to a 10 nm thick binding layer of chromium. A surface consisting of 12 nm of gold on top of 10 nm of chromium was coated with 300 nm of photoresist and then patterned using electron-beam lithography. The exposed photoresist was chemically removed and gold was then electroplated onto the surface. Finally, the unexposed photoresist was chemically removed

and ion sputtering was used to remove the tops of the pillars and the Au plating base layer, leaving free-standing gold pillars on top of a conductive thin film of chromium. Individual nanopillars are cylindrical with a diameter of 100 nm and a height of 285 nm and are arranged in a cubic lattice with 250 nm pitch. The tops of the pillars become partially rounded during the plasma etching step. Figure 2a is a scanning electron microscope (SEM) image taken at 29.0° from the surface normal. The nanopillar shape and aspect ratio were chosen phenomenologically, based on previous observations in the literature[1,17,18], such that the SPR along the long axis of the nanopillar (parallel to the TOF axis) is resonant within the laser bandwidth. Dark-field scattering measurements of individual nanopillars from a sample with larger pitch (4 μm) but otherwise prepared identically show a broadband plasmon resonance (Figure 2b), centered near 700 nm, that is well overlapped with the laser bandwidth. The broadening of around 0.2 eV is influenced both by radiative and nonradiative damping processes[19].

Control experiments were performed on a commercially available 50 nm thick gold film coated onto a Si $\langle 111 \rangle$ wafer (Ted Pella #16012-G). The flatness of the Si wafer allows for a gold surface with only ≈2.5 nm root-mean-squared surface roughness, which is measured by atomic force microscopy. Because of a mismatch in momentum, laser photons cannot couple to a surface plasmon wave in a flat gold surface unless special excitation geometries such as the Kretschmann configuration are used[3,20]. Under the experimental geometry presented here, no coupling should occur and plasmon enhanced effects should not be observed from this sample. Independent measurements of the damage threshold of the gold surface were made by raising the laser intensity to the point where photoelectron spectra collected at lower intensities were no longer reproducible. Measurements presented here are collected below the damage threshold[31].

III. RESULTS AND DISCUSSION

A. Photoelectron Spectra

In order to determine the interaction of ionized photoelectrons with the surface plasmon field, photoelectron kinetic energy spectra are recorded as a function of the excitation laser intensity. The few-cycle laser pulse is used to excite the plasmon resonance and si-

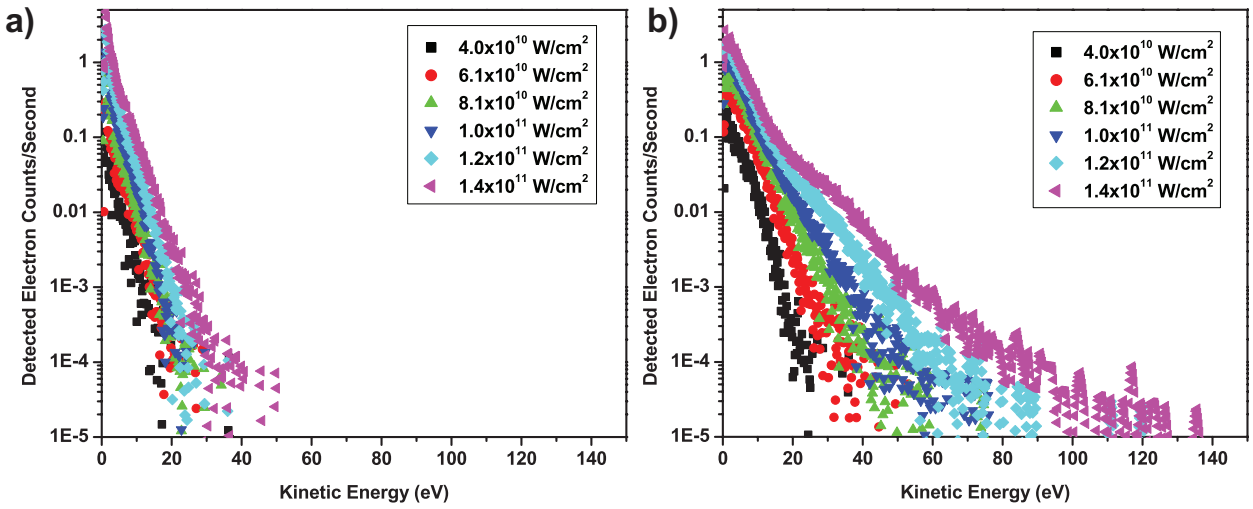

FIG. 3: (a) Photoelectron kinetic energy spectra taken from a flat gold surface as a function of excitation intensity. (b) Photoelectron spectra taken from the gold nanopillars at the same intensities as (a). Strong acceleration of photoelectrons to high kinetic energies is indicative of photoelectron emission in the presence of plasmon-enhanced electric fields. Because of the inability of photons to directly excite a SPR in flat gold, a minimal increase in kinetic energy is present in (a).

multaneously inject photoelectrons by nonlinear photoemission into the enhanced plasmon electric field. The work function of polycrystalline gold ranges from 4.7 eV to 5.2 eV[21]. The broadband laser pulse has $< 7 \times 10^{-3}$ intensity in the spectral range below 527 nm (half of 4.7 eV), therefore photoemission should require at least three laser photons to eject an electron into the continuum, even at the high energy side of the laser bandwidth. The excitation intensity is varied using a variable neutral density (ND) filter, the dispersion of which is pre-compensated by chirped mirrors. The laser pulse energy is measured at each intensity step and is used along with the pulse duration and the measured focal spot size to determine the intensity. Scanning the variable ND filter does not produce a detectable change in pulse duration, which is monitored by second-order interferometric autocorrelation. By decreasing or increasing the excitation intensity, the plasmon electron oscillation in the nanopillars can be driven more weakly or more strongly, respectively. We expect this change in field strength to result in varying degrees of acceleration experienced by photoelectrons injected into the plasmon field.

Figure 3a shows a series of photoelectron spectra taken from the reference flat gold sample

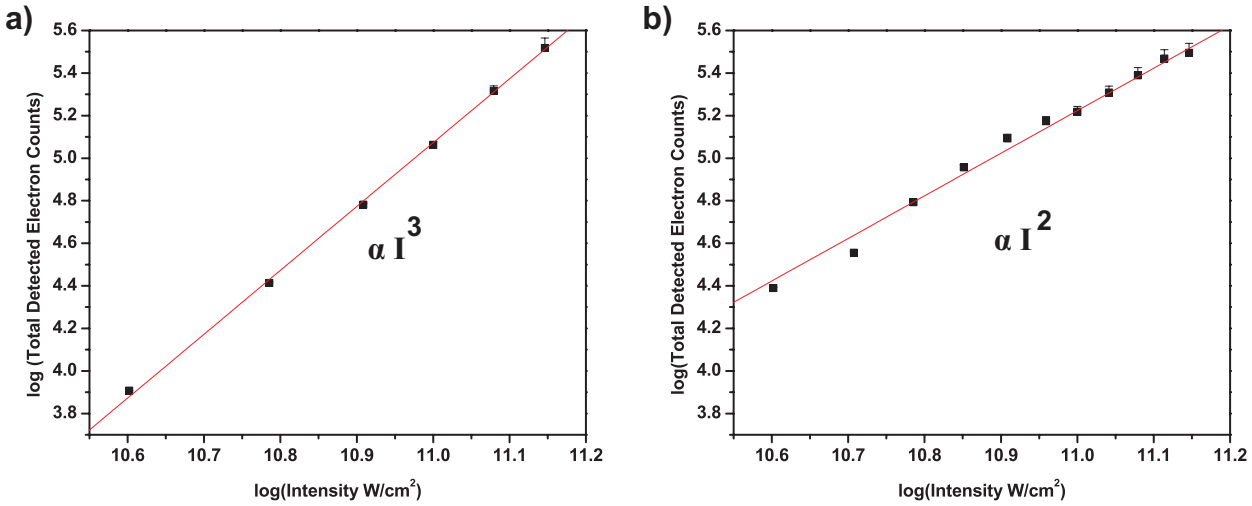

FIG. 4: Log-log plot showing the total number of detected photoelectrons as a function of excitation intensity, I, for (a) the flat gold surface and (b) the gold nanopillar sample. While the flat gold surface demonstrates the expected third order multiphoton dependence, only a second-order dependence is observed in emission from the nanopillars.

as a function of excitation intensity. Each spectrum is integrated over 60000 laser pulses. As previously noted, a plasmon oscillation cannot be directly excited on the flat gold surface by the laser because of the momentum mismatch between the laser photons and the surface plasmon resonance, therefore there should be no field enhancement. Figure 3b shows a similar series of photoelectron spectra taken from the gold nanopillar sample. As the laser intensity is increased, the maximum kinetic energy measured increases substantially and an increasingly strong secondary peak is formed between 10 eV and 40 eV. The shape of the spectral distribution is not significantly altered when corrected for missed electron counts due to the detector pulse-pair resolution. The dramatically increased electron kinetic energy with increasing excitation intensity in the nanopillars compared to the minimal increase at the same intensities in the flat gold spectra strongly suggests an enhanced plasmon-field-based acceleration mechanism. To further investigate the details of this mechanism we consider both the ionization and the acceleration processes in the following sections.

B. Total Electron Emission Scaling with Laser Intensity

To determine what effect the nanopillar SPR has on the photoelectron ionization process, a measurement is made of the total number of electrons detected as a function of the excitation intensity. Figure 4 shows the integrated photoelectron yield versus laser excitation intensity, I, for both samples on a log-log scale. Only the electrons emitted within the TOF angle of acceptance are detected, not absolute electron yield, thus only the relative scaling factors are considered and not the absolute electron yield between the two samples. The error bars are determined by the probability of missing electron counts during the detection electronics pulse-pair resolution dead-time. The data are the same as is shown in Figure 3 but with additional data points that are not displayed in Figure 3 for clarity. In both the nanopillar case and the flat gold case, a linear slope fits the observed trend, suggesting multiphoton ionization where the slope of such a fit results in a n^{th} order intensity dependence, where n is the number of photons required to exceed the work function of the metal[11]. Figure 4a shows the measured photoionization intensity dependence for the flat gold surface. In the flat gold case the expected I^3 dependence is observed, indicating a three photon multiphoton ionization process and no plasmon enhancement. Instead, in the case of gold nanopillars, Figure 4b, we observe a suppressed intensity dependence that only scales as I^2. This might be taken to suggest two-photon ionization, but such a process is implausible since the work function of the Au nanopillars would have to be unphysically low.

Previous observations have shown that it is possible to have a transition from the multiphoton ionization regime to the tunnel or mixed ionization regime caused by the enhanced plasmon field[7,13,15]. The relevant regime of photoemission for a given excitation intensity is typically described by the Keldysh parameter[22]:

$$\gamma = \sqrt{\frac{I_p}{2U_p}} \tag{1}$$

where I_p is the ionization potential of the target (W_f in the case of a solid) and U_p is the ponderomotive potential, given by:

$$U_p = \frac{e^2 E_0^2}{4m\omega_0^2} \tag{2}$$

where e is the elementary electric charge, E_0 is the electric field strength in V/m, m is

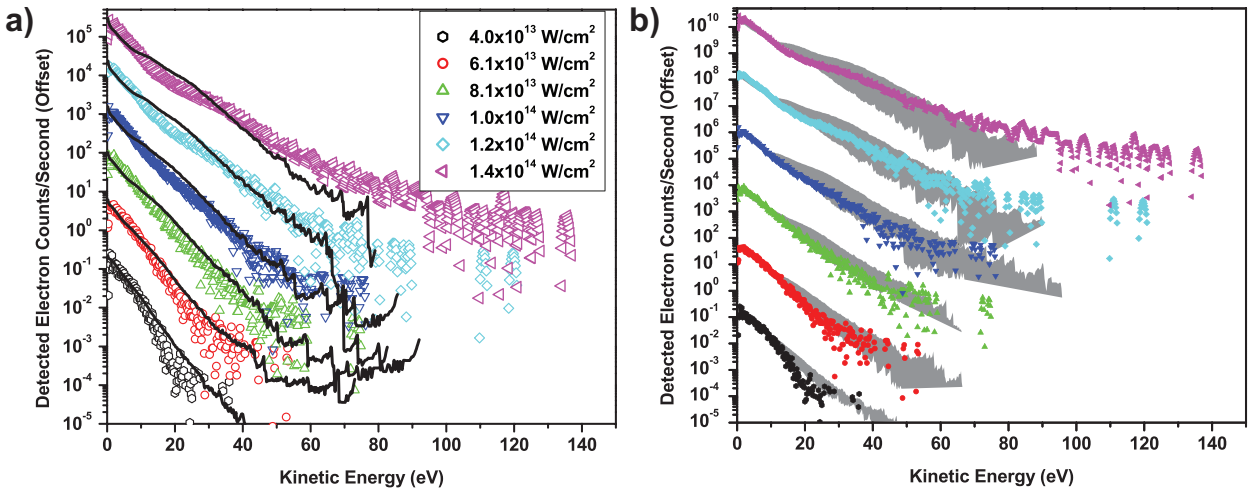

FIG. 5: (a) Spectra modeled from classical electron trajectory calculations (black lines) compared to the experimental data (symbols). Each trace is offset by one order of magnitude from the previous trace for clarity. In the model, nonlinear photoemission is followed by classical acceleration in an enhanced field. An average field enhancement of 32 brings the model in close agreement with the experimental data. The intensities shown in the legend are the enhanced intensity values, ($I \propto E^2$), used for the calculation. The experimental data is the same as shown in Figure 3b. (b) The experimental data (symbols) compared to a range of modeled spectra calculated for average field enhancement factors from 25-39 (shaded areas). Each trace and shaded area is offset by two orders of magnitude from the previous trace for clarity.

the electron mass, and ω_0 is the angular frequency of the laser electric field. For $\gamma >> 1$ multiphoton ionization is the primary mechanism, while for $\gamma << 1$ tunnel ionization tends to dominate.

At the maximum laser intensity of 1.4×10^{11} W/cm^2 used to irradiate the flat gold surface in our measurements, we find that $\gamma = 18$. This corresponds to electron emission firmly in the multiphoton regime, agreeing with the measured three photon dependence. Instead, the reduced slope observed for the nanopillars indicates strong-field ionization beyond the multiphoton regime, due to barrier suppression and tunneling ionization ($\gamma < 1$), suggesting a more than 18-fold field enhancement.

C. Classical acceleration model

The acceleration of the electrons in the plasmon field is modeled using a one dimensional classical electron trajectory calculation. In this calculation 1000 electrons are released into the enhanced electric field of a 7 fs FWHM Gaussian laser pulse at every time step, which are spaced by 4.8 as, resulting in a total of 7.5 million electrons[32]. The frequency of the enhanced field is assumed to be the same as the frequency of the laser pulse. Models of multiphoton photoemission from crystalline surfaces require sophisticated theoretical treatment and often produce significantly varying results[23]. A full calculation of nonlinear ionization from a metal surface is beyond the scope of this work; instead, initial electron kinetic energies are distributed according to a log-normal fit to the photoelectron spectra from the flat gold surface shown in Figure 3a. The amplitude of the log-normal fit is the only parameter varied for initial spectra at the different intensity values. After the initial release of electrons into the enhanced electric field, the position and velocity of each electron is calculated at each time step by integrating the classical equations of motion for a charged particle in an electric field. The final electron velocity as a function of ionization time, $v_f(t_i)$, is described by:

$$v_f(t_i) = v(t_i) + \int_{t_i}^{\infty} \frac{qE(t)}{m_e}\, dt \tag{3}$$

where $v(t_i)$ is the initial electron velocity, q is the elementary charge, m_e is the electron mass, and

$$E(t) = \frac{AE_0}{\sigma\sqrt{2\pi}} e^{-(t-a)^2/(2\sigma^2)} \cos(\omega t + \phi) \tag{4}$$

where A is the average electric field enhancement factor, E_0 is the peak value of the laser electric field, $\sigma = \mathrm{FWHM}/(2\sqrt{2\ln 2})$ with the FWHM laser pulse duration, a is the center of the Gaussian pulse, ω is the angular frequency of the electric field and ϕ is the carrier-envelope-phase (CEP) of the exciting laser pulse. The final electron velocity distribution as a function of electron ejection time is weighted by a temporal emission probability $\propto I(t)^2$, corresponding to a second-order nonlinear ionization process. Electrons with negative final velocity are excluded from the resulting spectrum because they would not reach the detector.

In our model, the spatial extent of the plasmon field is assumed to be significantly larger than the distance traveled by the electron while exposed to the plasmon field. Approximating the field as $1/r^3$, where r is the radius of the long nanopillar axis, one finds that the field decays to 1/10 of its value approximately 163 nm above the surface. By comparison, the

maximum electron excursion within the few-cycle pulse duration is only on the order of tens of nanometers.

However, because of the Gaussian spatial mode of the laser focus, not all ejected electrons will experience the peak intensity value. To account for this, the spectra presented here are constructed by integrating over individual spectra calculated at a range of intensity values over the spatial extent of the laser focus. The contributions from each spectrum are weighted according to the area illuminated by that intensity. In addition, these spectra are averaged for 5 values of the CEP over a range of 2π. The model is constructed as if the emission were from a flat surface (without nanostructures) with a uniform enhancement over the spatial profile of the laser pulse. In reality, the nanostructured surface will have an inhomogeneous field enhancement and ejected electrons will experience different fields. Additionally, the degree of coupling between localized plasmon modes is unknown at this time. The enhancement factor considered below represents an average of all of these possible inhomogeneities. The single free parameter in the calculation is therefore the average field enhancement factor due to the nanopillars, A, which is adjusted to give agreement between the observed and modeled photoelectron spectra. The same enhancement factor is applied to all of the spectra. The lifetime of the plasmon oscillation, phase-lag between the plasmon field and the exciting laser field, and surface recollision effects are not included in the calculation.

In order to directly compare the modeled spectra to all of the experimental data, the absolute electron yields of all the modeled spectra were scaled by a single value. This value is the ratio between the integrated photoelectron yield of the spectrum measured at the highest excitation intensity and the integrated photoelectron yield of the spectrum calculated at the highest enhanced intensity. This scaling places the modeled traces on the same absolute scale as the measured data while preserving the relative scaling of the modeled spectra produced by the calculation.

Figure 5a shows the experimental nanopillar data (symbols) compared to the modeled spectra (black lines), where a field enhancement of 32 times the experimentally used field strength is chosen. The uncertainty in the enhancement factor is estimated to be ± 7 and is determined by qualitatively comparing spectra calculated at various enhancement values to the experimental data. Figure 5b shows the experimental data (symbols) compared to a range of spectra modeled with enhancement factors ranging from 25 to 39 (shaded areas).

Such enhancement factors are in agreement with the assertion in Section III B that, in the case of the nanopillars $\gamma < 1$, indicating a transition to the strong-field regime.

The calculated spectra qualitatively reproduce the main features of the experimental data. Post-ionization acceleration of photoelectrons in the enhanced electric field results in the shifting of electrons from the initial kinetic energy distribution to higher kinetic energies and the formation of a secondary maximum between 10 eV and 40 eV. The fact that the secondary maximum is stronger in the modeled spectra and offset by several eV from the experimental data may result from non-uniform acceleration of photoelectrons due to the inhomogeneity of the enhanced field across the nanostructured surface. In addition to the electron kinetic energies, the relative electron yields of the spectra modeled using second-order nonlinear emission at the enhanced excitation intensities match well to the experimentally observed yields. When combined with the evidence for plasmon-assisted ionization described previously, the results of this model support a two step process of plasmon-enhanced ionization followed by classical electron acceleration in a plasmon-enhanced field. In addition, surface rescattering effects are expected to contribute higher energy electrons to the spectra[24–26], and their exclusion from this calculation may result in the failure of the model at the highest observed kinetic energies. Moreover, plasmon dephasing rates, which may be dependent on the amplitude of the launching field, have not been accounted for and could account for deviations of the data from the model as a function of intensity at higher electron kinetic energies. Since only an average enhancement factor is used, and because the highest kinetic energies derive from the highest field regions of the nanopillars, it is also not surprising that deviations at high kinetic energies are observed. Previous calculations of thin-film propagating plasmon-enhanced electron acceleration that include a more detailed description of the surface plasmon field produce similar results as this simple model[8,27].

IV. CONCLUSIONS

In conclusion, we observe photoelectron kinetic energies in photoemission from lithographically prepared gold nanopillars that are consistent with electron acceleration in electric fields with average strengths between 25 and 39 times higher than the experimentally used laser field strengths. Reference measurements from a flat gold surface do not produce such high electron kinetic energies at the same excitation intensities. The presence of a

plasmon-induced field enhancement is further supported by analysis of the excitation intensity dependence of the total electron emission yield. Total electron emission yields are observed for both the flat gold surface and the nanopillar sample, with the expected three-photon ionization process for the flat gold, but with a reduced photon dependence from the nanopillars indicative of a transition to the strong-field regime due to plasmon-enhanced electric fields. Classical electron trajectory calculations support the concept that the electrons are first ionized via plasmon-enhanced ionization and then subsequently accelerated in the enhanced electric field of the nanopillars to high kinetic energies.

These results provide the basis for the possibility of SPR-enhanced attosecond streaking from localized plasmon resonances in nanostructured surfaces. Such a concept has been explored theoretically for both nanostructures[28] and roughened metal surfaces[29]. In such an experiment, the attosecond streak camera scheme[30] would be modified to utilize the plasmon-enhanced electric field as a probe instead of the intense few-cycle laser pulse. Electrons are emitted by an isolated attosecond pulse in the presence of a plasmon field that has been excited by the femtosecond pump pulse. As the electrons are emitted their momentum will be changed by interaction with the sum of the plasmon field and the laser field. By taking advantage of the SPR field enhancement, it may be possible to reduce the contribution of the laser field itself sufficiently that information on the SPR lifetime and dynamics of the oscillating SPR electrons can be obtained directly from the electron momentum distribution. Given the observation of a significant field enhancement and multi-eV streaking of photoelectrons presented here, we expect that attosecond streaking studies of plasmon dynamics in metal nanostructures is possible.

V. ACKNOWLEDGEMENTS

Time-of-flight studies were supported by the NSF Division of Chemistry under award #CHE-0742662 [PMN, SRL] and by the Materials Sciences and Engineering Division of the U.S. Department of Energys Office of Basic Energy Sciences (DOE-BES) under Contract No. DE-AC02-05CH11231 [JSR, RAK]. Simulations were supported by the DOE-BES Chemical Sciences, Geosciences, and Biosciences Division, while nanopillar synthesis was performed under a user proposal at the Molecular Foundry, both under the above DOE contract. Few-cycle instrumentation development was supported by the AFOSR-MURI program under

award #FA95500410242. SRL gratefully acknowledges the support of a Department of Defense National Security Science and Engineering Faculty Fellowship (NSSEFF). TP and MJA also acknowledge a Max-Planck Research Group grant and a Alexander von Humboldt Foundation fellowship, respectively.

---

* Electronic address: RAKaindl@lbl.gov

† Electronic address: srl@berkeley.edu

[1] S. Eustis and M. A. El-Sayed, Chem. Soc. Rev. **35**, 209 (2006).

[2] U. Kreibig and M. Vollmer, *Optical Properties of Metal Clusters*, vol. 25 of *Springer Series in Materials Science* (Springer, 1995).

[3] H. Raether, *Surface plasmons on smooth and rough surfaces and on gratings*, vol. 111 of *Springer Tracts in Modern Physics* (Springer-Verlag, 1988).

[4] A. Campion and P. Kambhampati, Chem. Soc. Rev. **27**, 241 (1998).

[5] F. Sonvico, C. Dubernet, P. Colombo, and P. Couvreur, Curr Pharm Design **11**, 2091 (2005).

[6] S. Nie and S. Emory, Science **275**, 1102 (1997).

[7] S. Irvine and A. Elezzabi, Appl. Phys. Lett. **86**, 264102 (2005).

[8] S. Irvine and A. Elezzabi, Phys. Rev. A **73**, 013815 (2006).

[9] S. Irvine, A. Dechant, and A. Elezzabi, Phys. Rev. Lett. **93**, 184801 (2004).

[10] J. Kupersztych, P. Monchicourt, and M. Raynaud, Phys. Rev. Lett. **86**, 5180 (2001).

[11] J. Kupersztych and M. Raynaud, Phys. Rev. Lett. **95**, 147401 (2005).

[12] M. Raynaud and J. Kupersztych, Phys. Rev. B **76**, 241402 (2007).

[13] P. Dombi, S. E. Irvine, P. Racz, M. Lenner, N. Kroo, G. Farkas, A. Mitrofanov, A. Baltuska, T. Fuji, F. Krausz, et al., Opt Express **18**, 24206 (2010).

[14] P. Rácz, S. E. Irvine, M. Lenner, A. Mitrofanov, A. Baltuška, A. Y. Elezzabi, and P. Dombi, Appl. Phys. Lett. **98**, 111116 (2011).

[15] R. Bormann, M. Gulde, A. Weismann, S. V. Yalunin, and C. Ropers, Phys. Rev. Lett. **105**, 147601 (2010).

[16] C. Ropers, D. R. Solli, C. P. Schulz, C. Lienau, and T. Elsaesser, Phys. Rev. Lett. **98**, 043907 (2007).

[17] M. Pelton, J. Aizpurua, and G. Bryant, Laser Photonics Rev **2**, 136 (2008).

[18] K. Ueno, S. Juodkazis, V. Mizeikis, D. Ohnishi, K. Sasaki, and H. Misawa, Opt Express **15**, 16527 (2007).

[19] C. Sönnichsen, T. Franzl, T. Will, G. von Plessen, and J. Feldmann, Phys. Rev. Lett. **88**, 077402 (2002).

[20] E. Kretschmann and H. Raether, Z Naturforsch Pt A **A 23**, 2135 (1968).

[21] R. Lawson and G. Carter, Appl. Phys. Lett. **9**, 85 (1966).

[22] L. Keldysh, Sov Phys Jetp-Ussr **20**, 1307 (1965).

[23] F. Faisal and J. Kaminski, Phys Rev A **58**, R19 (1998).

[24] S. Zherebtsov, T. Fennel, J. Plenge, E. Antonsson, I. Znakovskaya, A. Wirth, O. Herrwerth, F. Süßmann, C. Peltz, I. Ahmad, et al., Nature Physics **4**, 1 (2011).

[25] G. Paulus, W. Becker, W. Nicklich, and H. Walther, Journal of Physics B: Atomic, Molecular and Optical Physics **27**, L703 (1994).

[26] M. Krüger, M. Schenk, and P. Hommelhoff, Nature **475**, 78 (2011).

[27] P. Dombi, P. Racz, and B. Bodi, Laser Part Beams **27**, 291 (2009).

[28] T. Pfeifer, M. J. Abel, P. M. Nagel, A. Jullien, Z.-H. Loh, M. J. Bell, D. M. Neumark, and S. R. Leone, Chemical Physics Letters **463**, 11 (2008).

[29] M. I. Stockman, M. F. Kling, U. Kleineberg, and F. Krausz, Nature Photon **1**, 539 (2007).

[30] J. Itatani, F. Quere, G. Yudin, M. Ivanov, F. Krausz, and P. B. Corkum, Phys. Rev. Lett. **88**, 173903 (2002).

[31] In the plotted intensity range, all spectra were reproducible. Significant modifications and non-reproducibility were, however, observed when increasing the intensity about one order of magnitude above the highest intensity reported in this work.

[32] The number of electrons used in the calculation is not made to match the experimentally detected electron counts and is only selected to obtain sufficiently resolved theoretical spectra.

DISCLAIMER